POPULATION OF HIGH SPIN STATES IN RELATIVISTIC FRAGMENTATION*

M. PFÜTZNER,

Institute of Experimental Physics, Warsaw University
Hoża 69, 00-681 Warsaw, Poland

P.H. REGAN, P.M. WALKER, ZS. PODOLYÁK, M. CAAMAÑO

Dept. of Physics, University of Surrey
Guildford, GU2 7XH, UK

J. GERL, M. HELLSTRÖM, P. MAYET

GSI, Planckstrasse 1, D-64291 Darmstadt, Germany

AND M.N. MINEVA

Div. of Cosmic and Subatomic Physics, Lund University
SE-22100, Sweden

for the GSI ISOMER Collaboration

(Received April 24, 2001)

The population probabilities of isomeric states in the 10 ns to ms regime have been studied following their production via the fragmentation of a ^{208}Pb beam at 1 GeV per nucleon. Gamma decays from approximately 20 isomeric states, mostly in the $A \sim 180$ region, have been measured. Their corresponding isomeric ratios were compared with theoretical predictions based on the abrasion–ablation model of fragmentation, which appears to provide an upper limit for the measured population probabilities as a function of angular momentum.

PACS numbers: 25.70.Mn, 27.80.+w

* Invited talk presented at the *High Spin Physics 2001* NATO Advanced Research Workshop, dedicated to the memory of Zdzisław Szymański, Warsaw, Poland, February 6–10, 2001.

1. Introduction

Progress in exploration of nuclei with extreme N/Z ratios, observed in the last decade (see for example Refs. [1–3]) profited to a large extend from the technique of projectile fragmentation at intermediate and relativistic energies, combined with the unambiguous channel selection afforded by state of the art magnetic separators and in-flight identification of individual ions. As recently demonstrated by results from both GANIL and GSI, the application of this technique to the spectroscopy of μs isomer decays, allows the first identification of excited states in nuclei very far from stability, even with secondary beam production rates as low as a few ions per minute [4,5].

However, rather surprisingly, one of the key variables in this method, namely the population of high-spin states in fragmentation reactions, has not been thoroughly studied. Recently, isomeric ratios of a number of microsecond isomers produced at GANIL in the quasifragmentation reaction of ^{112}Sn and ^{86}Kr beams were published [6,7] followed by a systematical measurement of the population of angular momentum at energies of about 60 MeV/nucleon [8]. However, for projectile energies above 100 MeV/nucleon, the only reported results are population probabilities for a few isomers produced at GSI Darmstadt [9,10].

A more systematic study of microsecond isomers has recently been performed at SIS/FRS facility at GSI with a beam of ^{208}Pb at 1 GeV/nucleon. Some results, including observation of a number of new isomers and isotopes as well as the discussion of selected cases, have already been published elsewhere [5,11–13]. In the current work we report on population probabilities deduced for approximately twenty previously known isomeric states which were identified in this experiment. A detailed description of the experiment and data analysis, and their comparison with the theoretical model described below, is given in Ref. [14]. In the present work, a brief summary of the main results and the question of the dependence of the isomeric ratios on the parallel momentum of the fragmentation products will be addressed.

2. Experimental considerations

Investigated nuclei were produced by the fragmentation of a 1 GeV per nucleon ^{208}Pb primary beam, delivered by the SIS synchrotron, impinging on a 1.6 g/cm^2 beryllium target, located at the entrance of the GSI projectile fragment separator FRS [15]. The average beam intensity varied between 1×10^6 and 2×10^8 ions per spill, depending on the setting of the FRS. The spill length and the repetition period were typically 4 and 10 s, respectively.

The FRS was operated in the standard achromatic mode with an aluminium wedge-shaped degrader of 4.4 g/cm^2 thickness located at the intermediate focal plane. Downstream of the target and the degrader niobium

foils of thickness 221 mg/cm^2 and 108 mg/cm^2, respectively, were mounted in order to increase the electron stripping efficiency. As the result, the typical probability of an ion being fully stripped was found to be about 96 % and 88 % for the two strippers, respectively.

The full in-flight identification of ions arriving to the final focal plane of the FRS was achieved by measurements of the magnetic rigidity ($B\rho$), time of flight (TOF) and energy loss (ΔE) of each ion. Two, 5 mm thick, plastic scintillators mounted at the intermediate and the final focal plane served for both the TOF and the horizontal position measurements. The latter, together with the magnetic field values, yielded the magnetic rigidity $B\rho$ of the particles. The horizontal position at the final focal plane was additionally measured by means of two multi-wire proportional chambers. The position at the final focus was used as a measure of the energy lost by an ion in the materials at the intermediate focal plane. Additional ΔE information was provided by an ionization chamber.

After passing the identification set-up, ions were slowed down in an aluminium degrader of variable thickness to be implanted in a 4 mm thick aluminium catcher. An additional plastic scintillator mounted in front of the catcher was used to suppress events resulting from nuclear interactions of ions during the slowing-down process. The catcher was surrounded by four segmented clover germanium detectors from the EXOGAM collaboration [16] and a large volume GSI 'Super Clover'. Each detector consisted of 4 separate germanium crystals but out of 16 available gamma channels only 14 were used — two channels were rejected due to bad performance.

The main steps in the heavy ion identification procedure are illustrated in Fig. 1 showing a sample of data collected while the FRS was optimized for the transmission of the fully stripped ^{191}W. First, from the $B\rho$ and TOF values the mass-to-charge ratio A/q is calculated. Then, the horizontal position at the intermediate focal plane, x_1, is plotted against A/q (Fig. 1(a)). The three distinctive groups of ions correspond to three charge state differences between the first and the second FRS sections. The group marked by a polygon represents ions which picked-up one electron while passing materials at the intermediate focus. They consist predominantly of fully stripped ions in the first section (target-to-degrader) and H-like in the second section (degrader-to-final focus). On the other hand, the group to the left of those, represents ions whose charge state remained unchanged while passing intermediate focus. These are mostly ions which passed the whole FRS as fully stripped ions. For events selected by the polygon in Fig. 1(a), the plot of horizontal position at the final focus, x_2, against A/q reveals individual elements and isotopes (Fig. 1(b)). As an example, events corresponding to ^{200}Pt are marked by a polygon shown in Fig. 1(b). Such selection is further

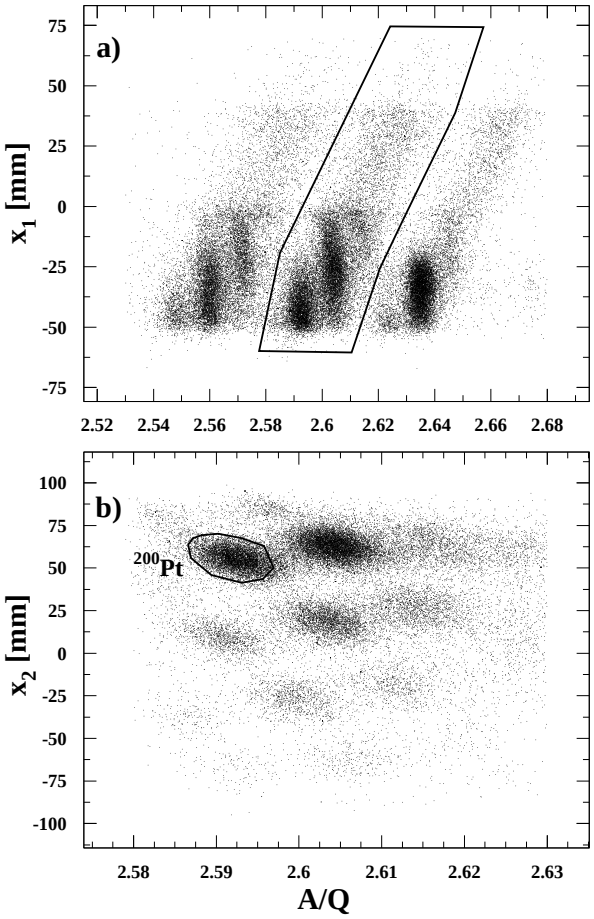

Fig. 1. Illustration of heavy ion identification procedure. (a) Horizontal position at the intermediate focus vs. A/q ratio measured at the second stage of the FRS. A contour line shows the selection of ions which picked-up one electron while passing materials at the intermediate focus. (b) Horizontal position at the final focus *vs.* A/q for ions selected in (a). Events corresponding to ^{200}Pt are indicated by a contour line.

purified by means of energy loss signals from the ionization chamber and the scintillator in front of the catcher. For the detailed description of the full procedure, the reader is referred to Ref. [14].

For each ion identified at the final focal plane, the electronic gate for gamma detection was opened for a period of 80 μs and all subsequent signals from gamma detectors, prompt and delayed, together with the signals from particle detectors were stored as a single event. For each channel, the gamma ray energy as well as the time between the implantation and gamma

detection was registered. The duration of the gate was much shorter than the average time between consecutive ions. Thus, delayed gamma radiation can be unambiguously associated with the identified ion. Such a gamma spectrum, correlated with ^{200}Pt events and summed over all detectors, is shown in Fig. 2. Gamma lines originating from the 7^- isomer [17] are clearly seen. The half-life of this isomer is only 14 ns, yet it survives the 300 ns flight through the separator. Since the energy of the isomeric transition in this case is lower than the K-electron binding energy, the conversion branch is blocked even in the H-like charge state and, consequently, the half-life of the highly stripped ion in flight is much longer than that of neutral atom at rest.

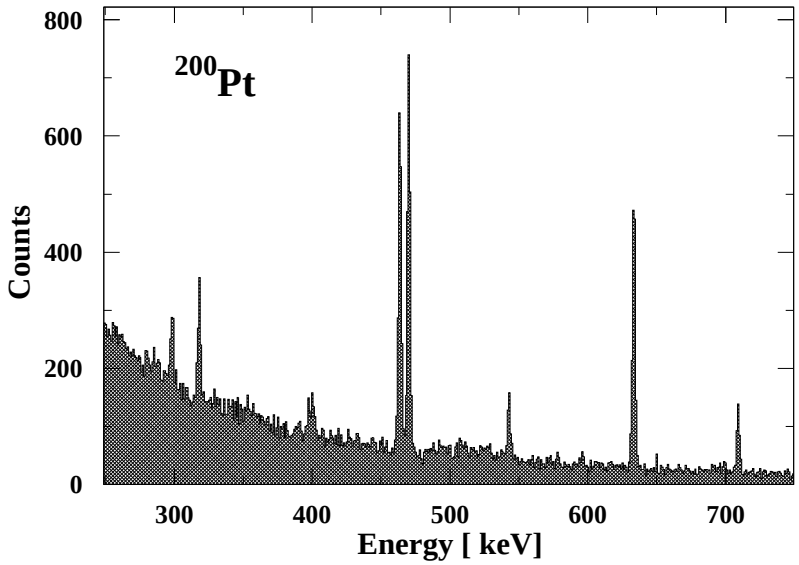

Fig. 2. Singles gamma spectrum corresponding to ^{200}Pt ions summed over 14 Ge-crystals. The time condition was applied that a gamma ray was detected less than 200 ns after the arrival of the ion including the prompt radiation.

The stopping of heavy ions in the catcher was accompanied by a burst of prompt radiation. Since the detection of prompt rays was allowed, and only the first gamma ray in every channel was recorded, the efficiency for delayed radiation was significantly reduced. This problem is illustrated in Fig. 3 where the multiplicity distribution of prompt gamma events correlated with ^{179}W ions is shown. It is seen that on average about 9 detectors out of 14 detected a prompt gamma ray less than 400 ns after arrival of a ^{179}W ion. This means that the effective efficiency for gamma rays delayed more than 400 ns is reduced in this case nearly by a factor of 3.

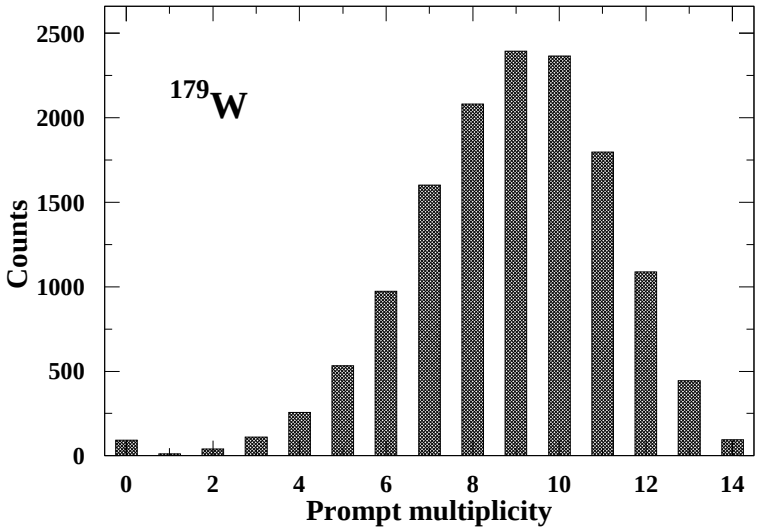

Fig. 3. Observed germanium detector multiplicity distribution of gamma rays detected less than 400 ns after arrival of a ^{179}W ion.

For the quantitative analysis of isomeric decays, the efficiency of each crystal as measured with calibration sources was corrected for this prompt-blocking effect. This correction was done separately for each selected isotope and for each crystal and involved calculating probabilities for detecting a prompt gamma ray.

3. Analysis and results

In the course of the experiment, decays of about 20 previously known isomers were detected. For these cases, where details of the isomer's decay scheme are known, one can determine the isomeric ratio, defined as the probability of populating the isomeric state in a given nucleus. The isomeric ratio R can be expressed in the following way:

$$R = \frac{N_\gamma \, (1 + \alpha_{\mathrm{tot}})}{N_{\mathrm{imp}} \, \varepsilon_{\mathrm{eff}} \; b_\gamma \, F \, G} \, , \tag{1}$$

where N_γ is the number of counts in the gamma line depopulating the isomer of interest, α_{tot} is the total conversion coefficient for this transition, $\varepsilon_{\mathrm{eff}}$ is the effective efficiency, b_γ is the probability that the decay proceeds through this transition (*i.e.*, the absolute branching ratio), N_{imp} is the number of implanted heavy ions, and F and G are correction factors for the in-flight isomer decay losses and for the finite detection time of gamma radiation,

respectively. The factor F is given by:

$$F = \exp\left[-\lambda^0 \left(\frac{\mathrm{TOF}_1}{\gamma_1} + \frac{\mathrm{TOF}_2}{\gamma_2}\right)\right], \tag{2}$$

where TOF_1 (TOF_2) is the Time Of Flight through the first (second) stage of the FRS, γ_1 (γ_2) is the corresponding Lorentz factor ($\gamma = 1/\sqrt{1-\beta^2}$). It is assumed here that ions are fully stripped in both stages of the FRS. Then their in-flight decay constant λ^0 could differ considerably from the value for an electrically neutral atom, λ. For the fully stripped ion the relation is:

$$\lambda^0 = \lambda \sum_i \frac{b_{\gamma i}}{1+\alpha^i_{\mathrm{tot}}}, \tag{3}$$

where the summation is over all the decay branches depopulating the isomer. If the analyzed gamma spectrum is produced with the delay-time values between t_i and t_f, the correction factor G is equal to:

$$G = \exp(-\lambda\, t_i) - \exp(-\lambda\, t_f)\,. \tag{4}$$

The results of this analysis are shown in Fig. 4 where the deduced isomeric ratios are plotted as a function of spin J. The data cover a broad range of angular momentum from $5\,\hbar$ to $35/2\,\hbar$. The latter value is presently the highest discrete angular momentum observed in a product of the fragmentation reaction.

The measured isomeric ratios are compared with a simple prediction based on the abrasion–ablation model of the fragmentation reaction. As shown by de Jong, Ignatyuk and Schmidt [18], the probability that the fragmentation product is formed in an initial state of angular momentum J can be approximated by a simple analytical formula:

$$P_J = \frac{2J+1}{2\sigma_f^2} \exp\left[-\frac{J(J+1)}{2\sigma_f^2}\right], \tag{5}$$

where σ_f, the so called spin-cutoff parameter, is given by:

$$\sigma_f^2 = 0.0178 \left(1 - \frac{2}{3}\beta\right) A_p^{2/3} \frac{\Delta A\,(3A_p - \Delta A)}{A_p - 1}\,. \tag{6}$$

A_p denotes the projectile mass number, ΔA is the mass difference between the projectile and the fragment and β is the quadrupole deformation parameter. The approximation holds for $\Delta A \geq 10$ and fails for fragments close to the projectile.

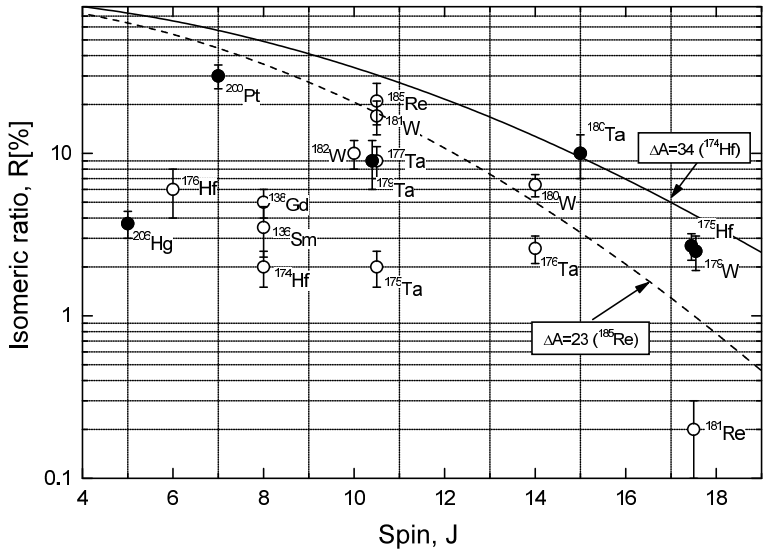

Fig. 4. Measured isomeric ratios as a function of isomer's spin J in units of $\hbar$. The full points indicate yrast states. Predictions of the simple sharp cut-off model are shown for two values of mass difference between the projectile and the isomer. In cases where two or more isomers were observed in the same nucleus, only the uppermost state is considered here.

Now, the probability that a statistical gamma cascade depopulating this initial state will lead to an isomeric state of spin J_m can be considered. We adopt an extreme simplifying assumption, known as the 'sharp cut-off' approximation, that all states with $J \geq J_m$, and only those, will decay to the isomer. This lead to the following prediction for the isomeric ratio:

$$R_{\mathrm{th}} = \int_{J_m}^{\infty} P_J \, dJ = \exp\left[-\frac{J_m \, (J_m + 1)}{2\sigma_f^2} \right] . \tag{7}$$

Since the predicted values depend not only on the spin of the isomer but also on its mass (via ΔA), no universal curve can be drawn in Fig. 4 to compare with the measured values. We observed however, that a majority of data points are from nuclei with masses between $A = 185$ and $A = 174$. Predictions for these two masses, assuming quadrupole deformation parameters of $\beta = 0.23$ [19], are shown in Fig. 4. We note that the sharp cut-off model appears to represent an upper limiting value for the isomeric ratio. The assumption that all states with the higher angular momentum decay to the isomer should rather overestimate the prediction, especially for

isomers lying far above the yrast line. Indeed, the yrast isomers, marked in Fig. 4 with the full circles, are generally populated with larger probabilities and are in reasonable agreement with the model. The two exceptions are ^{206}Hg and ^{179}Ta. The former case, differing from the projectile only by two mass units, cannot be described by Eqs. (5) and (6). The reduction of the isomeric ratio in case of ^{179}Ta might be explained by the existence of a long-lived isomer ($T_{1/2}$ = 11 ms, $I^{\pi} = 21/2^{+}$) located just above the observed $21/2^{-}$ state [20] which may trap a substantial part of the gamma cascade. Consequently, the feeding of the $21/2^{-}$ isomer, observed in the relatively short time (< 80 μs) may be reduced. This suggests that although the excitation energy of the isomer with respect to the yrast line is of some importance for the population probability, the structural factors, like the presence of long-lived states or detailed branching scheme, particularly close to the yrast line where the level density is low, may strongly affect the final result in individual cases.

4. Dependence of isomeric ratios on the fragment momentum

A recent study of isomer population in fragmentation-like reactions at intermediate energy [8] revealed that for the fragments close to the projectile the isomeric ratios depend strongly on the momentum of the fragment with a pronounced extremum value at the momentum of the beam. On the other hand, for fragments more than 6 nucleons away from the projectile no such dependence was found. Moreover, such a behavior was found to be in a qualitative agreement with the kinematical model of the fragmentation by Okuno *et al.* [21].

At relativistic energies the only result obtained prior to our work was the study of $19/2^{-}$ isomer in ^{43}Sc produced in the fragmentation of 500 MeV/nucleon ^{46}Ti beam [9]. Again, the very strong dependence on the momentum was found — in the wing of the momentum distribution the isomeric ratio was 15 times larger than in the center.

To search for similar phenomena in our data, we selected four cases where isomeric decays with high statistics were observed: two cases close to the projectile (^{206}Hg and ^{200}Pt) and two far from it (^{181}Re and ^{177}Ta). The information on the momentum of the fragment is given directly by the horizontal position at the intermediate (dispersive) focal plane, measured by the plastic scintillator. By imposing software cuts, events corresponding to different parts of the momentum distribution were selected and isomeric ratios were determined separately for each cut. The results of this analysis are shown in Fig. 5. Since the data acquisition was triggered by ions which arrived at the final focus, the observed yield distribution at the intermediate focal plane is cut by the FRS transmission. A comparison with the

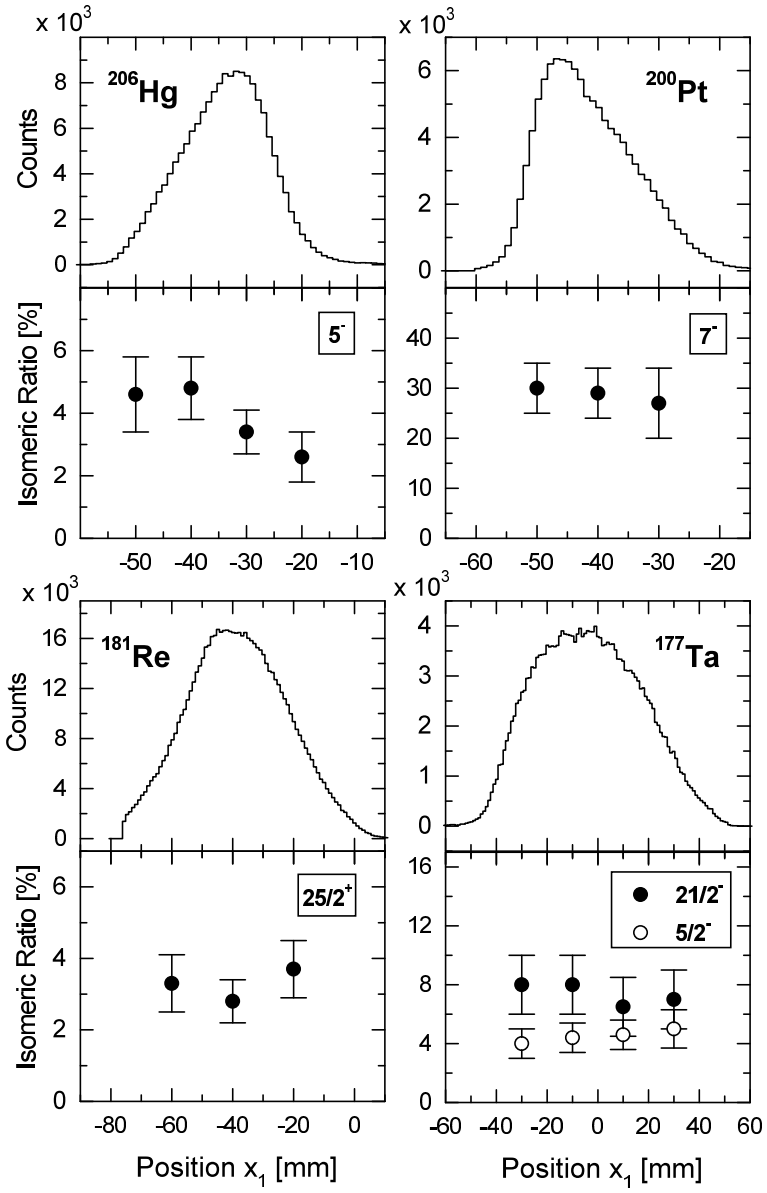

Fig. 5. Production yields (top) and isomeric ratios (bottom) for four nuclei measured as a function of horizontal position x_1 at the intermediate focal plane of the FRS which is proportional to the parallel momentum of the nucleus. The spin and parity of the analyzed isomer is indicated. The yield distributions for ^{206}Hg and ^{200}Pt are not symmetrical because they are cut by the FRS transmission.

ion-optical Monte Carlo simulations [22] showed that in case of ^{200}Pt approximately 80 % of the full momentum distribution is seen, while in other cases this number is larger than 90 %. Although the error bars are large, no strong dependence of isomeric ratio on the momentum (as reported in Refs. [8,9]) is observed. In case of ^{206}Hg, which is the closest nucleus to the projectile we have studied, an increase of isomeric ratio at low momentum is seen but it amounts only to about a factor of two.

5. Summary

The population of isomers produced in the relativistic fragmentation of a ^{208}Pb beam has been systematically investigated. Isomeric ratios were deduced for approximately 20 decays, in nuclei ranging is mass number from $A = 136$ up to $A = 206$, and up to $35/2\,\hbar$ in angular momentum. A simple theoretical prescription, based on the statistical abrasion–ablation model of the fragmentation mechanism was found to give a good representation of the upper limit for the isomer population probability. No clear dependence of the ratio on the momentum of the fragment was observed.

This work was supported by EPSRC (UK), the Polish State Committee for Scientific Research (KBN) under grant 2 P03B 036 15, Department of Energy contract DE-FG02-96ER40983 (USA), and the EU Access to Large Scale Facilities Programme.

REFERENCES

[1] R. Schneider *et al.*, *Z. Phys.* **A348**, 241 (1994).
[2] Ch. Engelmann *et al.*, *Z. Phys.* **A352**, 351 (1995).
[3] B. Blank *et al.*, *Phys. Rev. Lett.* **84**, 1116 (2000).
[4] J.M. Daugas *et al.*, *Phys. Lett.* **B476**, 213 (2000).
[5] Zs. Podolyák *et al.*, *Phys. Lett.* **B491**, 225 (2000).
[6] R. Grzywacz et.al., *Phys. Lett.* **B355**, 439 (1995).
[7] J.M. Daugas, Ph.D thesis, Université de Caen, Nov. 1999, unpublished, GANIL-T 99-05.
[8] J.M. Daugas *et al.*, *Phys. Rev.* **C63**, 064609 (2001).
[9] W.-D. Schmidt-Ott *et al.*, *Z. Phys.* **A350**, 215 (1994).
[10] M. Pfützner *et al.*, *Phys. Lett.* **B444**, 32 (1998).
[11] C. Schlegel *et al.*, *Phys. Scr. (T)* **88**, 72 (2000).
[12] M. Caamaño *et al.*, *Acta Phys. Pol.* **B32**, 763 (2001).
[13] M. Caamaño *et al.*, *Nucl. Phys.* **A682**, 223 (2001).

[14] M. Pfützner *et al.*, submitted to *Phys. Rev.* **C**.

[15] H. Geissel *et al.*, *Nucl. Instrum. Methods Phys. Res.* **B70**, 286 (1992).

[16] J. Simpson *et al.*, *Heavy Ion Physics* **11**, 159 (2000).

[17] S.Y. Yates, E.M. Baum, E.A. Henry, L.G. Mann, N. Roy, A. Aprahamian, R.A. Meyer, R. Estép, *Phys. Rev.* **C37**, 1889 (1988).

[18] M. de Jong, A.V. Ignatyuk and K.-H. Schmidt, *Nucl. Phys.* **A613**, 435 (1997).

[19] W. Nazarewicz, M.A. Riley, J.D. Garrett, *Nucl. Phys.* **A512**, 61 (1990).

[20] F.G. Kondev, G.D. Dracoulis, A.P. Byrne, T. Kibédi, S. Bayer, *Nucl. Phys.* **A617**, 91 (1997).

[21] H. Okuno *et al.*, *Phys. Lett.* **B335**, 29 (1994).

[22] N. Iwasa *et al.*, *Nucl. Instrum. Methods Phys. Res.* **B126**, 284 (1997).